

SoliReward: Mitigating Susceptibility to Reward Hacking and Annotation Noise in Video Generation Reward Models

Jiesong Lian^{1,†,*} Ruizhe Zhong^{2,†,*} Zixiang Zhou³ Xiaoyue Mi⁴
 Long Hu^{1,§} Yuan Zhou^{3,‡} Qinglin Lu³ Yixue Hao¹ Junchi Yan^{2,§}
¹Huazhong University of Science and Technology ²Shanghai Jiao Tong University
³Tencent Hunyuan ⁴University of Chinese Academy of Sciences

Abstract

Post-training alignment of video generation models with human preferences is a critical goal. Developing effective Reward Models (RMs) for this process faces significant methodological hurdles. Current data collection paradigms, reliant on in-prompt pairwise annotations, suffer from labeling noise. Concurrently, the architectural design of VLM-based RMs, particularly their output mechanisms, remains underexplored. Furthermore, RM is susceptible to reward hacking in post-training. To mitigate these limitations, we propose SoliReward, a systematic framework for video RM training. Our framework first sources high-quality, cost-efficient data via single-item binary annotations, then constructs preference pairs using a cross-prompt pairing strategy. Architecturally, we employ a Hierarchical Progressive Query Attention mechanism to enhance feature aggregation. Finally, we introduce a modified BT loss that explicitly accommodates win-tie scenarios. This approach regularizes the RM’s score distribution for positive samples, providing more nuanced preference signals to alleviate over-focus on a small number of top-scoring samples. Our approach is validated on benchmarks evaluating physical plausibility, subject deformity, and semantic alignment, demonstrating improvements in direct RM evaluation metrics and in the efficacy of post-training on video generation models. Code and benchmark are available at <https://github.com/lian700/SoliReward>

1. Introduction

Recent advancements in video generation models, such as Sora 2 [22], Veo 3 [7], and Seedance [6], have exhibited re-

markable capabilities in synthesizing high-fidelity, temporally coherent visual content. Behind these achievements, post-training alignment techniques, analogous to Reinforcement Learning from Human Feedback (RLHF) [23] in Large Language Models (LLMs), are becoming a key driving force for enhancing model performance and correcting physical implausibility, visual artifacts and instruction following. Currently, methods such as DanceGRPO [38] and LongChat-Video [27] have begun to utilize flow-based GRPO [16] methodologies to align video models.

However, the effectiveness of these alignment techniques relies heavily on the capabilities of their core component: the Reward Model (RM). RM is trained to quantify human preferences. However, constructing an RM that can accurately capture complex video qualities faces critical issues. These include data annotation noise and inconsistency, the vulnerability to reward hacking, and the under-explored design space for VLM-based RM architectures. On the data front, the dominant paradigm, pairwise preference learning [17], trains on video pairs (y_w, y_l) where y_w is preferred over y_l , typically using the Bradley-Terry (BT) loss [3]. While effective, this “in-prompt” annotation (pairing videos from the same prompt) struggles with pairs of comparable quality, where annotator ambiguity introduces substantial label noise. An alternative, point-wise scoring (e.g., using a five-level scale) [14], avoids direct comparison but introduces high inter-annotator disagreement due to the subjective and ambiguous nature of intermediate scores. This noise in the preference data fundamentally degrades the RM’s ability to accurately rank video quality. Beyond data noise, RM is highly susceptible to reward hacking in post-training, where the learned proxy objective deviates from intended human preferences [25]. Finally, the architecture used to extract this scalar reward is often insufficiently expressive, leading to a collapse of the reward where scores cluster together. Common methods, such as using the last token’s embedding [40], relying on the output of a dedicated special token [17], or using the probability of a “yes/no” token [34], may fail to capture the full spectrum of

¹† Work done during internship at Tencent Hunyuan.

²* Equal contribution.

lian700@hust.edu.cn, zerzerzer271828@sjtu.edu.cn

³‡ Project leader.

⁴§ Corresponding author. hulong@hust.edu.cn, yanjunchi@sjtu.edu.cn

information, from low-level artifacts to high-level semantic alignment, encoded across the model’s layers.

To mitigate these challenges, we propose a systematic framework towards robust video reward model training, including data annotation, training strategy and model architecture. We reorient data collection, shifting from complex relative comparisons or ambiguous multi-level scores towards simple, low-noise **single-item binary annotations** (Pass / Fail) targeting specific quality dimensions. To leverage the ranking ability of BT loss with these binary labels, we introduce a **cross-prompt pairing strategy**, where videos within one pair could belong to different prompts. This strategy generates a large-scale, high-signal preference dataset from simple binary labels, circumventing the noise inherent in ambiguous in-prompt comparisons.

Furthermore, we propose the BT with Win-Tie (BT-WT) loss to alleviate the critical issue of reward hacking [25]. By augmenting standard win-lose pairs with ‘win-tie’ pairs (e.g., pairing two ‘Pass’ samples), it explicitly penalizes score variance within the positive set, forcing the RM to map all high-quality samples to a compact manifold and thus mitigating reward spikes that lead to hacking.

Finally, to address the architectural limitations identified in extracting a reward signal from a VLM [1] backbone, we move beyond simplistic pooling strategies. We propose the **Hierarchical Progressive Query Attention (HPQA)**, a novel architecture that explicitly aggregates and refines features from multiple transformer layers, fusing low-level visual fidelity with high-level semantic understanding for a more robust reward signal. Our contributions are as follows:

- **On the data level**, we design a highly efficient and low-noise pipeline combining single-item binary annotation with a novel cross-prompt pairing strategy.
- **For the training objective**, we introduce BT-WT loss to enhance data efficiency and demonstrably mitigate reward hacking by balancing positive sample distributions.
- **Architecturally**, we propose the **HPQA**, a new reward model architecture that fuses multi-layer features for a more robust scalar reward.
- Finally, we establish new benchmarks for evaluating video generation quality based on **subject deformity** and **physical plausibility**, and demonstrate through extensive experiments that our combined framework surpasses existing RM training and architectural baselines.

2. Related Works

2.1. Data Construction for Reward Model Training

The efficacy of a Reward Model is fundamentally constrained by its training data. Existing annotation paradigms generally fall into three categories: pairwise comparisons, point-wise scoring, and binary annotation.

Pairwise Preference Annotation. The dominant

paradigm in RLHF [23] and recent video RMs [11, 20] involves querying preferences between two generations from the *same* prompt. This naturally aligns with BT objectives [3], which excel at modeling relative utility. However, in-prompt annotation suffers from severe decisional ambiguity when candidates exhibit similar quality levels. It forces subjective tie-breaking, injecting noticeable noise. While some efforts introduce “tie” options [17], defining standardized thresholds for neutrality remains difficult and does not fully resolve the underlying ambiguity.

Point-wise Scoring Annotation. Alternatively, discrete multi-level Likert scales (e.g., VideoScore [9]) could introduce high-variance labeling noise, particularly at subjective decision boundaries. As human preference is intrinsically continuous [39], forcing rigid discrete labels onto borderline samples (e.g., ‘3’ vs. ‘4’ for similar inputs) discards uncertainty and creates artificial quality gaps. This limitation is underscored by VideoScore [9], which reports critically low Inter-Annotator Agreement (IAA) (e.g., Fleiss’ $\kappa < 0.1$ [5] in Trial 2). We attribute this poor agreement to these boundary inconsistencies.

Binary Annotation. Recent work such as VisionReward [37] demonstrates that simplifying tasks to **binary** checklists achieves annotation consistency ($\sim 89\%$ agreement). However, its BT-objective is confined to learning linear weights, degenerating the reward into discrete scores and lacking the ranking granularity of more general RMs [17]. Our work bridges this critical gap.

2.2. Architecture of Reward Model

Vision Language Models (VLMs) [1] have emerged as the primary architectural choice for reward models, such as [9, 17, 20, 34, 37]. Commonly, a Vision Transformer processes visual inputs, mapping them into the language embedding space. A language backbone then uniformly processes these visual representations alongside textual inputs. However, the methodology for extracting a scalar reward score from the VLM’s output representations remains an open question. Three primary approaches are commonly employed to derive this score:

Linear Head [40]. This method utilizes the embedding of the *last token* from the VLM’s final hidden state, which is then fed into a Multi-Layer Perceptron (MLP) to produce the scalar score.

Special Token Head [17]. A dedicated special token (e.g., $\langle VQ \rangle$, $\langle MQ \rangle$, $\langle TA \rangle$ in VideoAlign) is prepended to the input sequence. The score is constructed by selectively isolating and extracting the logits from these pre-defined special token positions, with each token’s output mapping directly to a specific reward dimension.

Token Probability [34]. This method reframes the task as a prompted binary decision. The VLM is instructed to evaluate whether the visual input meets specific criteria and

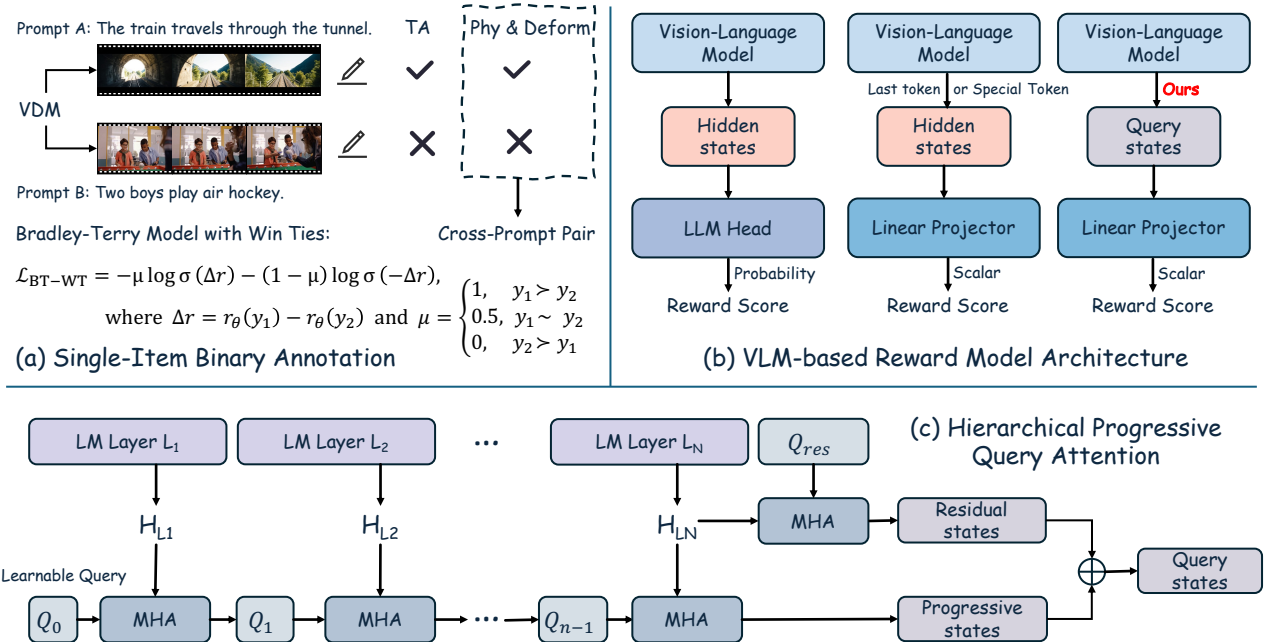


Figure 1. Pipeline of SoliReward, our framework for data annotation and training of video reward models. (a) We introduce a single-item binary annotation method, coupled with a cross-prompt pairing strategy, to mitigate annotation noise. Furthermore, to alleviate reward hacking, we propose the Bradley-Terry with Win-Tie (BT-WT) loss. (b/c) We propose a novel VLM-based Reward Model (VLM-RM) architecture, featuring a Hierarchical Progressive Query Attention (HPQA) adapter. This adapter progressively aggregates multi-level representations from the VLM backbone to compute a robust reward score.

to respond with a binary answer (e.g., “yes” or “no”). The reward is then extracted from the probability/logits assigned to the “yes” token in the model’s output.

2.3. Post-Training on Visual Generation

Aligning generative models with human preferences is a considerable challenge. The standard paradigm, RLHF, first trains a RM on human preferences and then fine-tunes the generative policy to maximize the RM’s score.

Group Relative Policy Optimization. Adapted for visual generation, GRPO-based online algorithms [13, 16, 19, 38, 42] addresses the instability of standard policy gradient methods. They utilize online feedback from reward model as guidance for optimization. By introducing Brownian motion, the ordinary differential equation (ODE) inherent in flow matching [15] is transformed into a stochastic differential equation (SDE). This infusion of stochasticity enhances the model’s exploration within the generation space.

Direct Preference Optimization. DPO [17, 18, 29, 35] offers an alternative to computationally intensive policy gradient methods by recasting the constrained RL objective as a classification problem. This reformulation simplifies the process, yielding a more stable training objective. RM can be leveraged to construct preference pairs for DPO training.

Reward Feedback Learning. ReFL [4, 21, 24, 36] is an alignment technique that utilizes a differentiable reward model, employing the reward signal directly as the

loss function. This mechanism allows for end-to-end optimization by backpropagating gradients from the reward model directly through the generative model’s parameters, thus avoiding the complexities of GRPO.

3. Methodology

In this section, we detail our pipeline. As shown in Fig. 1, we first introduce our data annotation approach (Sec. 3.1) and cross-prompt pairing strategy (Sec. 3.2). We then describe the training loss, a win-tie variant of the Bradley-Terry model (Sec. 3.3) designed to mitigate reward hacking and the reward model architecture HPQA (Sec. 3.4).

3.1. Data Annotation

The efficacy of an RM depends heavily on preference data quality, yet standard pairwise and point-wise methods suffer from high annotator ambiguity and disagreement [9, 17]. To mitigate this, we design a single-item binary annotation. By evaluating single videos against objective criteria (Pass/Fail), we diminish label noise and improve IAA, as shown in Sec. 4.1. We focus on three critical dimensions: **Physical Plausibility**, **Subject Deformity**, and **Semantic Alignment**. This binary scheme yields high-confidence signals. We annotate 250k in-house training videos and a 50k-video out-of-distribution (OOD) test set generated by other SOTA models. These samples originate from 20k unique prompts (please refer to Appendix Sec. 8 for details).

3.2. Cross-Prompt Pairing Strategy

Based on the high-quality binary labels from Sec. 3.1, we construct our preference data. We treat all samples within the ‘‘Pass’’ (W) set as mutually equivalent in preference ($\forall y_i, y_j \in W, y_i \sim y_j$). While ‘‘Fail’’ (L) samples may exhibit varying degrees of quality, every ‘‘Pass’’ sample is definitively preferred over every ‘‘Fail’’ sample ($\forall y_i \in W, \forall y_j \in L, y_i \succ y_j$). This establishes a clear preference order between the two sets.

Crucially, this formulation allows us to implement a cross-prompt pairing strategy. The Bradley-Terry model, upon which our loss is based, does not theoretically require pairs to originate from the same prompt [26]. By pairing ‘‘Pass’’ and ‘‘Fail’’ samples from different prompts, we create a large-scale, diverse dataset that forces the RM to learn generalized representations of quality rather than simple in-prompt relative rankings.

3.3. Bradley-Terry with Win-Tie

Reward model training relies on pairwise preference data. Given a pair (y_i, y_j) where y_i is preferred over y_j , the RM is commonly trained via the Bradley-Terry (BT) loss:

$$\mathcal{L}_{\text{BT}} = \mathbb{E}_{(y_i, y_j) \in D} [-\log(\sigma(r_\theta(y_i) - r_\theta(y_j)))] \quad (1)$$

However, during data annotation, annotators may deem two samples to have near-identical quality (i.e., ties, $y_i \sim y_j$). The vanilla BT loss discards these tie samples, reducing data efficiency. Furthermore, this win-lose only training scheme, particularly when annotating on specific dimensions, can induce reward hacking during subsequent model post-training [25]. Training exclusively on win-lose pairs seeks to maximize the reward margin $r_\theta(y_i) - r_\theta(y_j)$ in Eq. (1). Crucially, this objective imposes no constraints on the reward distribution *within* the set of positive samples.

This absence of constraint permits the RM to assign disproportionately high rewards to certain positive samples exhibiting shortcut features, while assigning relatively lower rewards to other valid positive samples that lack these artifacts. When a subsequent generative model explores this reward landscape, it preferentially converges to these reward spikes, learning to generate hacking-type samples. This exploitation of the RM’s scoring deficiencies to achieve high rewards, despite producing outputs that misalign with true human preferences, constitutes reward hacking.

Therefore, to mitigate reward hacking and improve data efficiency, we propose the Bradley-Terry with Win-Tie (BT-WT) strategy. We supplement the win-lose pairs $(y_i \succ y_j)$ with win-tie pairs $(y_i \sim y_j)$, which are constructed by pairing positive samples with other positive samples. Corresponding loss function is modified as follows, where W and L are the sets of positive and negative samples, respectively:

$$\begin{aligned} \mathcal{L}_{\text{BT-WT}} &= \mathbb{E}_{(y_i, y_j) \in W \times (W \cup L)} [-\mu \log \sigma(\Delta r) \\ &\quad - (1 - \mu) \log \sigma(-\Delta r)] \\ \Delta r &= r_\theta(y_i) - r_\theta(y_j), \mu = \begin{cases} 1, & y_i \succ y_j \\ 0.5, & y_i \sim y_j \end{cases} \end{aligned} \quad (2)$$

The fundamental mechanism by which these win-tie pairs mitigate reward hacking is the imposition of a regularization constraint on the RM’s output space. As shown in Eq. (2), the tie-loss component of $\mathcal{L}_{\text{BT-WT}}$ explicitly penalizes the reward discrepancy between any two positive samples. This loss term compels the RM to map all positive samples onto a **more compact and dense manifold** within the reward space, ensuring $r_\theta(y_i) \approx r_\theta(y_j)$. This mechanism acts as a regularizer, effectively flattening the spurious spikes in the reward landscape and promoting smoothness.

Consequently, RM provides a more robust and accurate optimization signal for the generative model. This guides the model to learn the generalizable features of high-quality samples, rather than exploiting the specific defects and loopholes of the reward model. As shown in Fig. 3, incorporation of win-tie sample pairs markedly alters the score distribution of positive samples, leading to a more concentrated distribution in the high-score segment. We also propose a test to evaluate a dimension’s suitability for win-tie pair construction, detailed in Sec. 6 in Appendix.

In contrast, VideoAlign [17] retains all tie samples and employs a loss function that operates on A-wins, B-wins, or a tie (including both win-tie and lose-tie pairs). We argue this strategy is unsuitable for our annotation scenario. Given two independently labeled negative samples (e.g., for deformity), we cannot assert their degree of deformity is equivalent. Erroneously pairing them as a tie would diminish the discriminative capacity of RM and degrade model performance.

3.4. Hierarchical Progressive Query Attention

We introduce Hierarchical Progressive Query Attention (HPQA), a novel reward model adapter architecture for computing the reward scalar from query states. HPQA computes rewards by aggregating features from multiple language model (LM) transformer layers. Let $H_i \in \mathbb{R}^{B \times S \times D}$ be the hidden state output of layer i , and $I = [l_1, l_2, \dots, l_N]$ be a list of N specified layer indices.

The operational flow begins by generating an initial query vector $q^{(1)} \in \mathbb{R}^{B \times 1 \times D}$. This is achieved by attending to the first specified hidden state H_{l_1} using a single, learnable query vector $q^{(0)} \in \mathbb{R}^{1 \times 1 \times D}$. This vector $q^{(0)}$ acts as the Query, while the input hidden state H_{l_1} serves as both the Key and Value in a standard Multi-Head Attention (MHA) operation:

$$q^{(1)} = \text{MHA}_1(Q = q^{(0)}, K = H_{l_1}, V = H_{l_1}) \quad (3)$$

Table 1. Inter-Annotator Agreement (IAA) analysis across 5 annotators. We report Krippendorff’s α [8], Fleiss’s κ [5] and raw agreement for our binary *single-item* task and *pair-wise comparison* task. Single-item is more consistent than pairwise annotation.

Annotation	α	κ	Agreement	Interpretation
Single-Item	0.4939	0.4925	0.7733	Moderate
Comparison	0.3516	0.3494	0.5467	Fair

The output $q^{(1)}$ is progressively refined over the subsequent $N - 1$ layers specified in I . For $i = 2$ to N , the MHA module at layer l_i takes $q^{(i-1)}$ as Query, using hidden state H_{l_i} as both Key and Value:

$$q^{(i)} = \text{MHA}_i(Q = q^{(i-1)}, K = H_{l_i}, V = H_{l_i}) \quad (4)$$

The final iteration’s resulting vector $q^{(N)}$ serves as the progressive feature q_{prog} . Concurrently, o_{res} is computed by attending to the last hidden state H_L via a separate attention module. This module uses another learnable query q_{res} as the Query, with H_L serving as both Key and Value:

$$o_{\text{res}} = \text{MHA}_{\text{res}}(Q = q_{\text{res}}, K = H_L, V = H_L) \quad (5)$$

These two vectors are combined via residual connection and passed to RewardHead to yield the final scalar reward r :

$$r = \text{RewardHead}(q_{\text{prog}} + o_{\text{res}}) \quad (6)$$

A primary advantage of this mechanism is its ability to create a rich feature representation by explicitly aggregating information hierarchically. This approach is conceptually grounded in findings from linguistic analysis in LLMs [28], which reveals that transformer layers exhibit functional specialization. For instance, their analysis indicates that attention aligns most strongly with syntactic dependency relations in the middle layers, while the deepest layers are most effective at capturing distant relationships. Our mechanism is designed to explicitly harness this hierarchical specialization. The progressive refinement Eq. (4) allows the model to synthesize a query that explicitly bridges these different semantic levels, fusing low-level fidelity with high-level abstraction. Furthermore, the residual connection ensures that this hierarchical information augments rather than replaces the representation from the final layer.

4. Experiments

In this section, we empirically evaluate our reward model on both in-domain and out-of-domain accuracy. Additionally, evaluations are demonstrated in post-training on text-to-video (T2V) task. We use the InternVL3 [43] series as the reward model backbone and HunyuanVideo [12] for post-training verification.

4.1. Data Annotation and Pairing Strategy

To validate the reliability of our single-item binary annotation approach against traditional pairwise comparisons, we

Table 2. Reward model accuracy compared to baselines. * means the score distribution degenerates to discrete values.

Task	Approach	RM ACC	
		ID	OOD
Phy & Deform	VideoScore [9]	62.30	67.09
	VideoScore-v1.1 [9]	60.20	68.65
	LiFT [32]	52.60*	61.11*
	VisionReward [37]	58.45	50.75
	VideoPhy [2]	67.35	65.10
	UnifiedReward [33]	49.90*	44.18*
	VideoAlign [17]	54.40	71.60
	Ours	78.48	80.08
TA	VideoScore [9]	52.75	54.05
	VideoScore-v1.1 [9]	51.20	53.36
	LiFT [32]	1.75*	7.40*
	VisionReward [37]	30.75*	22.24*
	VideoPhy [2]	54.85	60.52
	UnifiedReward [33]	16.45*	10.63*
	VideoAlign [17]	49.50	49.14
	Ours	79.02	60.25

conduct a formal Inter-Annotator Agreement (IAA) analysis, tasking 5 annotators to label a subset of data using both methods. In Tab. 1, we report Krippendorff’s α [8], Fleiss’s κ [5], and the raw percentage agreement. Our single-item task achieves a **Moderate** agreement, registering $\alpha = 0.4939$, $\kappa = 0.4925$, and a strong raw agreement of 77.33%. These results are substantially higher than those from the pairwise comparison task, which only reached **Fair** agreement ($\alpha = 0.3516$, $\kappa = 0.3494$) with a 54.67% raw agreement. It confirms that our point-wise annotation framework yields more consistent and reliable labels from annotators compared to the conventional pairwise approach.

Regarding the pairing strategy, a comparison between in-prompt and cross-prompt methods is deferred to Sec. 7.1 in Appendix (Tab. 7 and Tab. 8) due to page limitations. The cross-prompt strategy achieves performance comparable to its in-prompt counterpart, while also effectively leveraging data from prompts that yielded only a single video. This approach enhances data utilization without compromising reward model performance.

4.2. Reward Model

4.2.1. Evaluation of Accuracy

We benchmark the accuracy of SoliReward against representative baselines on both in-domain (ID) and out-of-domain (OOD) data. ID accuracy is measured on a held-out partition of our training dataset, which is unseen during training process. For OOD evaluation, we employ videos generated by state-of-the-art (SOTA) models (including Wan2.1 [30], Wan2.2 [30], Veo 3 [7] and Seedance 1.0 [6]) from a curated prompt set. Video quality is then assessed by human annotators across three criteria: Physical Plausibility, Subject Deformity (Phy & Deform), and

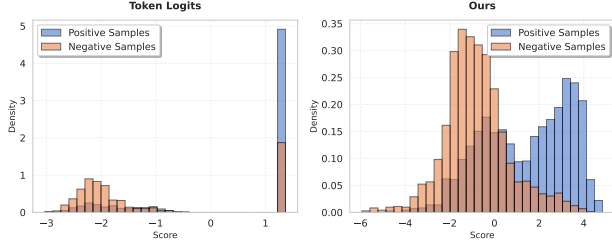


Figure 2. The reward score distributions on the semantic alignment task reveal that alternative architectures suffer from severe score clustering, assigning identical ratings to many samples.

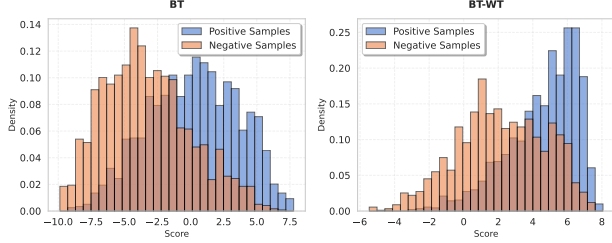


Figure 3. Reward distribution for BT and BT-WT. BT-WT contributes to a more concentrated distribution in the high-score segment for positive samples.

Semantic Alignment (TA). Evaluation on OOD dataset is critical [34] because ID accuracy is an insufficient indicator of downstream task performance. OOD accuracy, which assesses generalization capability on shifted distributions, serves as a more robust predictor of a model’s final efficacy. Consequently, OOD accuracy emerges as a more critical metric for evaluating a model’s true utility.

We present the reward model accuracy comparison in Tab. 2. Our model demonstrates substantially superior performance and generalization capability compared to existing baselines. For the **Phy & Deform** task, our model achieves the highest accuracy on both ID data (78.48) and OOD data (80.08). This surpasses all baselines, including the second-best model, VideoAlign (71.60). On the **TA** task, our model attains a dominant ID accuracy of 79.02, far exceeding the closest baseline, VideoPhy (54.85). Its OOD performance (60.25) is highly competitive, matching the top (VideoPhy, 60.52) and outperforming others.

Notably, several baselines (marked with *) that suffer from score clustering (e.g., LiFT, UnifiedReward). They output discrete scores, such as integers from 1-5 or categorical labels (good/normal/bad). This coarse granularity, coupled with their limited OOD generalization, causes score clustering: many samples are assigned identical ratings, thus deflating the accuracy.

4.2.2. Bradley-Terry with Win-Tie

Despite the reward models trained via BT and BT-WT exhibiting comparable accuracy, the BT-WT RM yields better performance during post-training (shown in Tab. 3). We an-

Table 3. Comparison of reward model performance trained via BT and BT-WT. Reward model accuracy and post-training evaluation metrics are reported.

Method	Reward Model	Post-Training	
	ACC	VBench2	MQ
BT	77.63	0.8693	0.1719
BT-WT	78.27	0.8999	0.3302

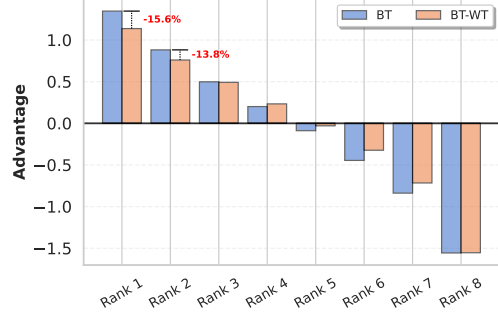


Figure 4. Intra-group advantage distribution in BT-WT exhibits smaller advantages for top-ranked samples compared to BT, thereby mitigating the over-optimization.

alyze this divergence from the following two perspectives.

Group Advantage. Our empirical observations confirm that group advantage from a standard BT-trained reward model exhibit larger absolute values than those from BT-WT-trained RM, especially in top-rank samples. Standard BT loss, seeking only to maximize the positive-negative margin within the high-quality samples. Consequently, during GRPO-based post-training leveraging group advantage, this RM assigns high-variance scores to samples of comparable quality within a group. This high variance in advantage calculation, $A_i = \frac{r_i - \bar{r}}{\sigma}$, leads to **over-optimization**: outlier samples with anomalously high scores generate massive positive advantages, causing the policy to overfit to non-generalizable features. The win-tie pairs in BT-WT act as a calibrator, compelling the RM to map high-quality samples to a more compact score interval. This results in smaller absolute advantage values, which precisely signifies lower gradient variance for more robust policy updates. Group advantage comparison between BT and BT-WT during post-training is shown in Fig. 4.

Regularization. From the perspective of regularization, the win-tie pairs function as a critical regularizer against reward hacking. An RM trained exclusively on win-lose pairs is prone to overfitting to shortcut features. This vulnerability is readily exploited during post-training: the policy network quickly identifies and leverages these spurious features to maximize corresponding reward, while achieving only limited improvements in perceptual video quality. The BT-WT paradigm, by introducing win-tie pairs, compels the RM to learn a more robust and generalizable internal repre-

Table 4. Comparison of reward models on post-training. HunyuanVideo is selected as the video generation backbone, and DanceGRPO algorithm is applied to fine-tune the model. VideoAlign MQ, our reward model score, and VBench2 Human Fidelity are selected as evaluation metrics.

Backbone	RM	MQ	SoliReward	VBench2
HunyuanVideo	-	-0.0980	4.5628	0.8426
HunyuanVideo	MQ	0.1607	4.8968	0.8695
HunyuanVideo	Ours	0.3302	5.3554	0.8999

Table 5. Comparison of reward model architecture. * means score clustering shown in Fig. 2, where the score distribution degenerates to discrete values.

Task	Approach	RM ACC	
		ID	OOD
Phy & Deform	Linear (Ln) [40]	74.69	78.66
	‘Yes’ token logits [34]	75.43	78.46
	Special token + Ln [17]	75.91	73.61
	HPQA (Ours)	78.48	80.08
TA	Linear (Ln) [40]	72.41*	31.92*
	‘Yes’ token logits [34]	71.56*	31.37*
	Special token + Ln [17]	76.25	58.38
	HPQA (Ours)	79.02	60.25

sensation aligned with human preferences. This paradigm constrains the RM to assign proximate scores to perceptually distinct yet high-quality samples. This constraint enhances the RM’s capacity to model the complex concept of human preference, making it less susceptible to reward hacking and yielding a more reliable optimization signal for post-training.

4.3. Post-Training

We conduct post-training to further validate our reward model on physical plausibility and subject deformity. HunyuanVideo [12] is selected as the video generation backbone. We apply online reinforcement learning post-training with DanceGRPO [38], guided by our reward model. This process enhances video quality in these two aspects. To quantify this, we employ the VideoAlign Motion Quality (MQ) [17] and VBench2 Human Fidelity [41] evaluation metrics. As shown in Tab. 4, the results confirm the efficacy of our reward model during this post-training phase.

To further demonstrate the necessity of our reward model, we conduct a comparative analysis against existing RMs, such as VideoAlign MQ. We perform a parallel post-training experiment using VideoAlign MQ as the sole guidance signal. As shown in Tab. 4 and Fig. 6, VideoAlign MQ fails to effectively mitigate videos exhibiting physical law violations or deformities. Visual comparisons confirm this: models optimized with VideoAlign MQ continue to generate such artifacts. In contrast, under identical settings, the model guided by our reward signal successfully alleviates these issues in Fig. 5. Furthermore, when evaluating the

Table 6. Impact of the BCE Penalty on Reward Model Accuracy and Score Margin. While accuracy is comparable, the BCE penalty significantly reduces the score margin, negatively impacting post-training.

Method		Reward Model		Post-Training	
BT-WT	BCE	ACC	Margin	VBench2	MQ
✓	✓	78.32	2.97	0.8826	0.1154
✓		78.48	3.72	0.8999	0.3302
	✓	75.99	1.75	-	-

post-trained models using our reward model, VideoAlign MQ, and VBench2 Human Fidelity as distinct metrics, our approach consistently outperforms the VideoAlign-guided baseline across all three dimensions. This substantiates our claim that existing MQ-focused reward models are insufficient for addressing physical plausibility and subject deformity, a critical gap our reward model successfully fills. Due to page limitation, post-training experiments on semantic alignment are demonstrated in Sec. 7.5.2 in Appendix.

4.4. Ablation Study

Model Architecture. We benchmark our HPQA against three common alternative architectures: 1) Extracting the last token embedding from the final hidden state and projecting it via a linear layer to derive a score; 2) VideoAlign [17], which introduces a special token placeholder in the model input and uses its corresponding output embedding, processed by a linear layer, as the score; and 3) RewardDance [34], which instructs the reward model to output ‘yes’ or ‘no’ and utilizes the predicted probability of the ‘yes’ token as the reward. As Tab. 5 indicates, our HPQA method outperforms the other architectures in terms of accuracy, validating its efficacy.

More critically, we observe that reward models based on these alternative architectures are highly susceptible to score clustering during training, particularly for semantic alignment. Specifically, the scores for positive and negative samples converge to several discrete values. This leads to an overly concentrated score distribution lacking sufficient diversity, consequently diminishing the model’s ability to discriminate between samples of varying quality. This ultimately impairs its guidance capabilities during post-training optimization. In contrast, our HPQA architecture does not suffer from this instability, remaining stable across diverse video quality evaluation dimensions. This demonstrates the robustness of our proposed architecture.

Binary Cross Entropy. RewardDance [34] augments the BT loss with a cross-entropy penalty during point-wise RM training. However, it does not thoroughly explore this component’s impact on RM accuracy and subsequent post-training performance. Motivated by this gap, we empirically investigate the effect of this binary cross-entropy (BCE) penalty, treating the RM’s output as logits for a bi-

A person with a red nose holds two Rubik's Cubes.

A woman sits at a desk with papers, holding up signs that say "LESSON 1" and "3+7"



Figure 5. Visual results guided by different reward models. From top to bottom: Baseline (HunyuanVideo), VideoAlign, and Ours.

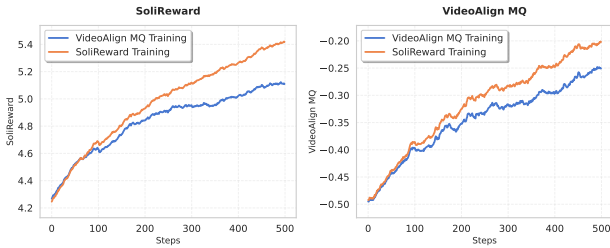


Figure 6. Comparison of reward scores between post-training guided by our reward model and VideoAlign MQ.

nary pass/fail task. The results reveal a critical insight. RM accuracy is a deceptive metric when decoupled from the reward margin. As shown in Tab. 6, adding the BCE penalty ('BT-WT + BCE') yields comparable accuracy to our 'BT-WT' baseline. However, this BCE-penalized RM leads to *inferior* post-training performance.

We hypothesize this failure stems from **reward margin degradation**. The BCE loss compels the RM to function as a binary classifier, collapsing the nuanced score spectrum into two discrete points (e.g., positive vs. negative). This classification focus overshadows the fine-grained ranking needed to distinguish between samples, compromising the model's ability to express relative preference. This hypothesis is strongly supported by Tab. 6. The 'BT-WT + BCE' model's reward margin (2.97) represents a 19.62% collapse compared to the standard 'BT-WT' model (3.72). Furthermore, a pure 'BCE' model yields the lowest margin of all. During post-training, a policy network generates videos with subtle quality differences. An RM with a col-

lapsed margin is blind to these nuances and thus incapable of providing the effective gradient signals needed for successful optimization. This finding underscores that a large, discriminative reward margin, not just classification accuracy, is a critical prerequisite for a successful reward model.

5. Conclusion and Future Work

We introduce SoliReward, a systematic framework for video reward model, including both data annotation and model training designed to mitigate annotation noise and reward hacking. It employs a scalable, low-noise, and cost-efficient single-item binary annotation scheme, enabling a robust cross-prompt pairing strategy that compels the RM to learn generalizable video quality representations. Technically, SoliReward features two key innovations: the Hierarchical Progressive Query Attention architecture, a reward adapter that fuses multi-level features, and the Bradley-Terry with Win-Tie loss to alleviate reward hacking. Experiments demonstrate SoliReward achieves superior RM accuracy and, crucially, translates these gains to improved post-training performance.

Limitation & Future Work. Future work can be extended to other conditional generation tasks, such as image-to-video (I2V). Besides, our reward model scores input videos along a single dimension, and multiple dimensions can be fused into a single RM by designing several learnable queries. We observe more performance gains when scaling our RM from 1B to 8B parameters, but diminishing returns when scaling further to 14B. This finding on model scaling highlights a key avenue for future exploration.

References

- [1] Shuai Bai, Keqin Chen, Xuejing Liu, Jialin Wang, Wenbin Ge, Sibao Song, Kai Dang, Peng Wang, Shijie Wang, Jun Tang, et al. Qwen2. 5-vl technical report. *arXiv preprint arXiv:2502.13923*, 2025. 2
- [2] Hritik Bansal, Zongyu Lin, Tianyi Xie, Zeshun Zong, Michal Yarom, Yonatan Bitton, Chenfanfu Jiang, Yizhou Sun, Kai-Wei Chang, and Aditya Grover. Videophy: Evaluating physical commonsense for video generation. *arXiv preprint arXiv:2406.03520*, 2024. 5
- [3] Ralph Allan Bradley and Milton E Terry. Rank analysis of incomplete block designs: I. the method of paired comparisons. *Biometrika*, 39(3/4):324–345, 1952. 1, 2
- [4] Kevin Clark, Paul Vicol, Kevin Swersky, and David J Fleet. Directly fine-tuning diffusion models on differentiable rewards. *arXiv preprint arXiv:2309.17400*, 2023. 3
- [5] Joseph L Fleiss and Jacob Cohen. The equivalence of weighted kappa and the intraclass correlation coefficient as measures of reliability. *Educational and psychological measurement*, 33(3):613–619, 1973. 2, 5
- [6] Yu Gao, Haoyuan Guo, Tuyen Hoang, Weilin Huang, Lu Jiang, Fangyuan Kong, Huixia Li, Jiashi Li, Liang Li, Xiaojie Li, et al. Seedance 1.0: Exploring the boundaries of video generation models. *arXiv preprint arXiv:2506.09113*, 2025. 1, 5, 3
- [7] Google. Veo 3 announcement. <https://blog.google/technology/ai/generative-media-models-io-2025/>, 2025. Accessed: September 29, 2025. 1, 5, 3
- [8] Andrew F. Hayes and Klaus Krippendorff. Answering the call for a standard reliability measure for coding data. *Communication Methods and Measures*, 1(1):77–89, 2007. 5
- [9] Xuan He, Dongfu Jiang, Ge Zhang, Max Ku, Achint Soni, Sherman Siu, Haonan Chen, Abhramil Chandra, Ziyang Jiang, Aaran Arulraj, et al. Videoscore: Building automatic metrics to simulate fine-grained human feedback for video generation. *arXiv preprint arXiv:2406.15252*, 2024. 2, 3, 5
- [10] Ziqi Huang, Yanan He, Jiashuo Yu, Fan Zhang, Chenyang Si, Yuming Jiang, Yuanhan Zhang, Tianxing Wu, Qingyang Jin, Nattapol Chanpaisit, et al. Vbench: Comprehensive benchmark suite for video generative models. In *Proceedings of the IEEE/CVF Conference on Computer Vision and Pattern Recognition*, pages 21807–21818, 2024. 4
- [11] Yuval Kirstain, Adam Polyak, Uriel Singer, Shahbuland Matiana, Joe Penna, and Omer Levy. Pick-a-pic: An open dataset of user preferences for text-to-image generation. *Advances in neural information processing systems*, 36:36652–36663, 2023. 2
- [12] Weijie Kong, Qi Tian, Zijian Zhang, Rox Min, Zuozhuo Dai, Jin Zhou, Jiangfeng Xiong, Xin Li, Bo Wu, Jianwei Zhang, et al. Hunyuanvideo: A systematic framework for large video generative models. *arXiv preprint arXiv:2412.03603*, 2024. 5, 7
- [13] Yuming Li, Yikai Wang, Yuying Zhu, Zhongyu Zhao, Ming Lu, Qi She, and Shanghang Zhang. Branchgrpo: Stable and efficient grpo with structured branching in diffusion models. *arXiv preprint arXiv:2509.06040*, 2025. 3
- [14] Youwei Liang, Junfeng He, Gang Li, Peizhao Li, Arseniy Klimovskiy, Nicholas Carolan, Jiao Sun, Jordi Pont-Tuset, Sarah Young, Feng Yang, et al. Rich human feedback for text-to-image generation. In *Proceedings of the IEEE/CVF Conference on Computer Vision and Pattern Recognition*, pages 19401–19411, 2024. 1
- [15] Yaron Lipman, Ricky TQ Chen, Heli Ben-Hamu, Maximilian Nickel, and Matt Le. Flow matching for generative modeling. *arXiv preprint arXiv:2210.02747*, 2022. 3
- [16] Jie Liu, Gongye Liu, Jiajun Liang, Yangguang Li, Jiaheng Liu, Xintao Wang, Pengfei Wan, Di Zhang, and Wanli Ouyang. Flow-grpo: Training flow matching models via online rl. *arXiv preprint arXiv:2505.05470*, 2025. 1, 3
- [17] Jie Liu, Gongye Liu, Jiajun Liang, Ziyang Yuan, Xiaokun Liu, Mingwu Zheng, Xiele Wu, Qiulin Wang, Menghan Xia, Xintao Wang, et al. Improving video generation with human feedback. *arXiv preprint arXiv:2501.13918*, 2025. 1, 2, 3, 4, 5, 7
- [18] Runtao Liu, Haoyu Wu, Ziqiang Zheng, Chen Wei, Yingqing He, Renjie Pi, and Qifeng Chen. Videodpo: Omni-preference alignment for video diffusion generation. In *Proceedings of the Computer Vision and Pattern Recognition Conference*, pages 8009–8019, 2025. 3
- [19] Yifu Luo, Penghui Du, Bo Li, Sinan Du, Tiantian Zhang, Yongzhe Chang, Kai Wu, Kun Gai, and Xueqian Wang. Sample by step, optimize by chunk: Chunk-level grpo for text-to-image generation. *arXiv preprint arXiv:2510.21583*, 2025. 3
- [20] Yuhang Ma, Xiaoshi Wu, Keqiang Sun, and Hongsheng Li. Hpsv3: Towards wide-spectrum human preference score. In *Proceedings of the IEEE/CVF International Conference on Computer Vision*, pages 15086–15095, 2025. 2
- [21] Xiaoyue Mi, Wenqing Yu, Jiesong Lian, Shibo Jie, Ruizhe Zhong, Zijun Liu, Guozhen Zhang, Zixiang Zhou, Zhiyong Xu, Yuan Zhou, et al. Video generation models are good latent reward models. *arXiv preprint arXiv:2511.21541*, 2025. 3
- [22] OpenAI. Sora 2. <https://openai.com/zh-Hans-CN/index/sora-2/>, 2025. Accessed: November 1, 2025. 1
- [23] Long Ouyang, Jeffrey Wu, Xu Jiang, Diogo Almeida, Carroll Wainwright, Pamela Mishkin, Chong Zhang, Sandhini Agarwal, Katarina Slama, Alex Ray, et al. Training language models to follow instructions with human feedback. *Advances in neural information processing systems*, 35:27730–27744, 2022. 1, 2
- [24] Xiangwei Shen, Zhimin Li, Zhantao Yang, Shiyi Zhang, Yingfang Zhang, Donghao Li, Chunyu Wang, Qinglin Lu, and Yansong Tang. Directly aligning the full diffusion trajectory with fine-grained human preference. *arXiv preprint arXiv:2509.06942*, 2025. 3
- [25] Joar Skalse, Nikolaus Howe, Dmitrii Krashennnikov, and David Krueger. Defining and characterizing reward gaming. *Advances in Neural Information Processing Systems*, 35:9460–9471, 2022. 1, 2, 4
- [26] Hao Sun, Yunyi Shen, and Jean-Francois Ton. Rethinking bradley-terry models in preference-based reward mod-

- eling: Foundations, theory, and alternatives. *arXiv preprint arXiv:2411.04991*, 2024. 4
- [27] Meituan LongCat Team, Xunliang Cai, Qilong Huang, Zhuoliang Kang, Hongyu Li, Shijun Liang, Liya Ma, Siyu Ren, Xiaoming Wei, Rixu Xie, et al. Longcat-video technical report. *arXiv preprint arXiv:2510.22200*, 2025. 1
- [28] Jesse Vig and Yonatan Belinkov. Analyzing the structure of attention in a transformer language model. *arXiv preprint arXiv:1906.04284*, 2019. 5
- [29] Bram Wallace, Meihua Dang, Rafael Rafailov, Linqi Zhou, Aaron Lou, Senthil Purushwalkam, Stefano Ermon, Caiming Xiong, Shafiq Joty, and Nikhil Naik. Diffusion model alignment using direct preference optimization. In *Proceedings of the IEEE/CVF Conference on Computer Vision and Pattern Recognition*, pages 8228–8238, 2024. 3
- [30] Team Wan, Ang Wang, Baole Ai, Bin Wen, Chaojie Mao, Chen-Wei Xie, Di Chen, Feiwei Yu, Haiming Zhao, Jianxiao Yang, et al. Wan: Open and advanced large-scale video generative models. *arXiv preprint arXiv:2503.20314*, 2025. 5, 3
- [31] Peng Wang, Shuai Bai, Sinan Tan, Shijie Wang, Zhihao Fan, Jinze Bai, Keqin Chen, Xuejing Liu, Jialin Wang, Wenbin Ge, et al. Qwen2-vl: Enhancing vision-language model’s perception of the world at any resolution. *arXiv preprint arXiv:2409.12191*, 2024. 2
- [32] Yibin Wang, Zhiyu Tan, Junyan Wang, Xiaomeng Yang, Cheng Jin, and Hao Li. Lift: Leveraging human feedback for text-to-video model alignment. *arXiv preprint arXiv:2412.04814*, 2024. 5
- [33] Yibin Wang, Yuhang Zang, Hao Li, Cheng Jin, and Jiaqi Wang. Unified reward model for multimodal understanding and generation. *arXiv preprint arXiv:2503.05236*, 2025. 5
- [34] Jie Wu, Yu Gao, Zilyu Ye, Ming Li, Liang Li, Hanzhong Guo, Jie Liu, Zeyue Xue, Xiaoxia Hou, Wei Liu, et al. Rewarddance: Reward scaling in visual generation. *arXiv preprint arXiv:2509.08826*, 2025. 1, 2, 6, 7
- [35] Ziyi Wu, Anil Kag, Ivan Skorokhodov, Willi Menapace, Ashkan Mirzaei, Igor Gilitschenski, Sergey Tulyakov, and Aliaksandr Siarohin. Densedpo: Fine-grained temporal preference optimization for video diffusion models. *arXiv preprint arXiv:2506.03517*, 2025. 3
- [36] Jiazheng Xu, Xiao Liu, Yuchen Wu, Yuxuan Tong, Qinkai Li, Ming Ding, Jie Tang, and Yuxiao Dong. Imagereward: Learning and evaluating human preferences for text-to-image generation. *Advances in Neural Information Processing Systems*, 36:15903–15935, 2023. 3
- [37] Jiazheng Xu, Yu Huang, Jiale Cheng, Yuanming Yang, Jiajun Xu, Yuan Wang, Wenbo Duan, Shen Yang, Qunlin Jin, Shurun Li, et al. Visionreward: Fine-grained multi-dimensional human preference learning for image and video generation. *arXiv preprint arXiv:2412.21059*, 2024. 2, 5
- [38] Zeyue Xue, Jie Wu, Yu Gao, Fangyuan Kong, Lingting Zhu, Mengzhao Chen, Zhiheng Liu, Wei Liu, Qiushan Guo, Weilin Huang, et al. Dancegrpo: Unleashing grpo on visual generation. *arXiv preprint arXiv:2505.07818*, 2025. 1, 3, 7
- [39] Zhiyuan You, Xin Cai, Jinjin Gu, Tianfan Xue, and Chao Dong. Teaching large language models to regress accurate image quality scores using score distribution. In *Proceedings of the Computer Vision and Pattern Recognition Conference*, pages 14483–14494, 2025. 2
- [40] Yuze Zhao, Jintao Huang, Jinghan Hu, Xingjun Wang, Yunlin Mao, Daoze Zhang, Zeyinzi Jiang, Zhikai Wu, Baole Ai, Ang Wang, et al. Swift: a scalable lightweight infrastructure for fine-tuning. In *Proceedings of the AAAI Conference on Artificial Intelligence*, pages 29733–29735, 2025. 1, 2, 7
- [41] Dian Zheng, Ziqi Huang, Hongbo Liu, Kai Zou, Yanan He, Fan Zhang, Lulu Gu, Yuanhan Zhang, Jingwen He, Wei-Shi Zheng, et al. Vbench-2.0: Advancing video generation benchmark suite for intrinsic faithfulness. *arXiv preprint arXiv:2503.21755*, 2025. 7, 2
- [42] Ruizhe Zhong, Jiesong Lian, Xiaoyue Mi, Zixiang Zhou, Yuan Zhou, Qinglin Lu, and Junchi Yan. Euphonium: Steering video flow matching via process reward gradient guided stochastic dynamics. *arXiv preprint arXiv:2602.04928*, 2026. 3
- [43] Jinguo Zhu, Weiyun Wang, Zhe Chen, Zhaoyang Liu, Shenglong Ye, Lixin Gu, Hao Tian, Yuchen Duan, Weijie Su, Jie Shao, et al. Internvl3: Exploring advanced training and test-time recipes for open-source multimodal models. *arXiv preprint arXiv:2504.10479*, 2025. 5

SoliReward: Mitigating Susceptibility to Reward Hacking and Annotation Noise in Video Generation Reward Models

Supplementary Material

6. More Discussions about BT-WT

While ‘pass’ can form win-ties in single-item annotation, the applicability is dimension-dependent. Binary annotation inherently compresses a continuous quality spectrum into two discrete points. For some dimensions, ‘pass’ denotes an absolute, discrete state. While for others, ‘pass’ merely signifies surpassing a subjective threshold, masking underlying gradations of quality. We propose a test to assess a dimension’s suitability:

Does a shared ‘pass’ label for samples y_i and y_j imply identical underlying quality, or merely a negligible difference?

Yes: The dimension is suitable for constructing win ties.
No (i.e., y_i may still be superior to y_j): The dimension is unsuitable for win ties.

7. Additional Experiments

7.1. Pairing Strategy

We ablate the impact of data pairing strategies on reward model performance by comparing two approaches: the in-prompt and cross-prompt pairing strategies. In the in-prompt method, both videos within a preference pair are generated from an identical prompt. Conversely, the cross-prompt strategy permits a pair to be formed from videos generated by different prompts. We construct separate training datasets using each strategy and evaluated the resulting RMs’ accuracy and reward margin on fixed evaluation datasets. As shown in Tab. 7 and Tab. 8, the cross-prompt strategy achieves performance comparable to its in-prompt counterpart. Furthermore, a hybrid strategy combining both datasets also yielded similar results. The primary advantage of the cross-prompt approach is its relaxed data requirement: while the in-prompt method necessitates two or more video generations per prompt, the cross-prompt strategy can effectively leverage data from prompts that yielded only a single video. This improves the utilization of available data without compromising reward model performance.

7.2. Model Scaling

As demonstrated in Tab. 9, our analysis of model scaling reveals two key findings. First, performance improvements are substantially more pronounced in the OOD evaluation than in the ID setting. Second, these scaling benefits are not monotonic and are heavily concentrated in the transition from 1B to 8B parameters. This initial scaling step yields

Table 7. Impact of pairing-strategy for reward model training. Accuracy is evaluated on both ID and OOD datasets. The cross-prompt strategy is comparable with in-prompt strategy.

Task	Approach	Reward ACC	
		ID	OOD
Phy & Deform	Cross-Prompt	76.74	79.54
	In-Prompt	76.77	79.22
	Hybrid	76.09	79.16
TA	Cross-Prompt	76.39	60.25
	In-Prompt	76.67	59.26
	Hybrid	75.64	59.41

Table 8. Impact of pairing-strategy for reward model training. Pair score margin is evaluated on both ID and OOD datasets. The cross-prompt strategy is comparable with in-prompt strategy.

Task	Approach	Reward Margin	
		ID	OOD
Phy & Deform	Cross-Prompt	3.83	4.17
	In-Prompt	3.98	3.77
	Hybrid	3.98	4.13
TA	Cross-Prompt	2.93	1.47
	In-Prompt	2.73	1.28
	Hybrid	2.87	1.37

Table 9. Influence of model size on reward model accuracy and reward margin between positive and negative samples.

Task	Approach	ID		OOD	
		ACC	Margin	ACC	Margin
Phy & Deform	InternVL3-1B	76.25	3.10	77.65	2.95
	InternVL3-8B	78.48	3.60	81.43	5.51
	InternVL3-14B	78.57	3.69	81.71	5.19
TA	InternVL3-1B	77.48	2.08	58.45	0.33
	InternVL3-8B	79.02	2.11	63.46	0.92
	InternVL3-14B	78.83	2.15	65.29	0.71

significant OOD accuracy gains (up to +5.01) and dramatically improves the OOD reward margin (e.g., from 2.95 to 5.51 for “Phy & Deform”), whereas ID accuracy sees only modest increases. In contrast, scaling further from 8B to 14B yields diminishing returns.

The observed diminishing returns when scaling from 8B to 14B parameters, following significant gains from 1B to 8B, suggest a multi-faceted bottleneck. The initial 1B model is likely under-parameterized, lacking the capacity to capture essential features, which the 8B model successfully acquires. However, the 8B model may already achieve

Table 10. Comparison of reward model performance trained via BT, BTT and BT-WT. Reward model accuracy and VBench2 Human Fidelity scores are reported.

Method	Reward Model	Post-Training	
	ACC	VBench2	MQ
BT	77.63	0.8693	0.1719
BTT	77.78	0.8700	0.0690
BT-WT	78.27	0.8999	0.3302

capacity saturation for the given task’s intrinsic complexity. This means the additional parameters of the 14B model offer only marginal utility. Furthermore, performance is likely becoming data-limited, where the 14B model requires a larger or more diverse dataset than available to unlock further gains. This is supported by the degradation in the OOD reward margin for both tasks, which indicates the 14B model may be overfitting to the training data, a common challenge when model size outpaces data scale and optimization refinement.

7.3. BT, BTT and BT-WT

We evaluate the impact of the BT, Bradley-Terry with Ties (BTT), and BT-WT loss functions on RM training and subsequent policy optimization. The three losses utilize different data pairing strategies: BT uses only win-lose pairs; BTT incorporates win-lose, win-tie, and lose-tie pairs; and BT-WT employs win-lose and win-tie pairs. The BTT data consists of the BT-WT data plus an additional 150k lose-tie pairs.

As discussed in Sec. 3.3, VideoAlign [17] retains all tie samples, using a loss function that models A-wins, B-wins, or ties (which includes both win-tie and lose-tie pairs). We contend this approach is ill-suited for our annotation scenario. Specifically, if two negative samples are labeled independently (e.g., for deformity), we cannot assume their degree of severity is equivalent. Erroneously treating them as a ‘tie’ (a lose-tie pair) would introduce label noise, diminishing the RM’s discriminative capacity and ultimately degrading policy performance.

Empirical results in Tab. 10 support this argument: BTT achieves a lower RM accuracy than BT-WT. Furthermore, the degradation extends to generation quality. As shown in the post-training metrics, the BTT approach results in inferior VBench2 Human Fidelity scores compared to BT-WT. These findings confirm that incorporating lose-tie pairs into the loss function is suboptimal for our data distribution.

7.4. HPQA Layer Indices

Empirical results in Table 11 and Table 12 demonstrate that the HPQA architecture maintains its efficacy across diverse VLM backbones. Furthermore, our ablation study indicates that aggregating representations from 4 to 5 intermediate layers yields better performance.

Table 11. Performance of Qwen2-VL (2B) [31] across different layer indices.

Task	Layer Indices	ID		OOD	
		ACC	Margin	ACC	Margin
Phy & Deform	‘Yes’ Token	75.40	1.71	77.05	1.69
	{14, 28}	75.79	1.71	77.24	1.85
	{9, 18, 28}	75.20	1.64	77.59	1.59
	{7, 14, 21, 28}	76.34	1.72	77.78	1.81
	{6, 12, 18, 24, 28}	76.29	1.77	78.89	1.84
TA	{5, 10, 14, 19, 23, 28}	74.11	1.67	75.73	1.56
	‘Yes’ Token	77.33	3.41	55.28	0.70
	{7, 14, 21, 28}	78.62	3.55	56.19	0.56
	{5, 10, 14, 19, 23, 28}	77.53	3.17	56.33	0.54

Table 12. Performance of Qwen2.5-VL (3B) and InternVL3 (14B) across different layer indices.

Task	Model	Layer Indices	ID		OOD	
			ACC	Margin	ACC	Margin
Phy & Deform	Qwen2.5-VL (3B)	‘Yes’ Token	75.45	1.61	40.76*	-1.52*
		{9, 18, 27, 36}	73.68	1.61	76.38	1.50
		{7, 14, 21, 28, 36}	73.51	1.47	76.61	1.39
		{6, 12, 18, 24, 30, 36}	72.87	1.43	74.27	1.35
		{16, 32, 48}	78.10	3.56	80.99	5.39
InternVL3 (14B)	{12, 24, 36, 48}	78.50	3.52	80.31	5.17	
	{9, 18, 27, 36, 48}	78.20	3.71	81.16	5.21	
	‘Yes’ Token	76.19	1.89	27.73*	0.24*	
TA	Qwen2.5-VL (3B)	{9, 18, 27, 36}	76.54	2.84	59.06	0.51
		{6, 12, 18, 24, 30, 36}	77.23	2.80	58.16	0.35

* scores degenerate to discrete values.

Table 13. Comparison of different approaches on human preference benchmarks from VBench2 [41]. The evaluation metrics include Anatomy (Human Anatomy), Clothes (Human Clothes), Identity (Human Identity), and Fidelity (Human Fidelity).

Method	Anatomy	Clothes	Identity	Fidelity (Overall)
Baseline	0.8915	0.8905	0.7457	0.8426
VideoAlign-MQ	0.9009	0.8714	0.8361	0.8695
‘Yes’ Token w/ BT	0.9154	0.9067	0.7778	0.8666
‘Yes’ Token w/ BT-WT	0.9312	0.9259	0.8013	0.8861
HPQA w/ BT	0.9153	0.9064	0.7861	0.8693
HPQA w/ BTT	0.9254	0.8922	0.7923	0.8700
HPQA w/ BT-WT	0.9164	0.9231	0.8601	0.8999

7.5. Post-Training

7.5.1. Physical Plausibility and Subject Deformity

We select corresponding VBench2 Human Fidelity, including human anatomy, human clothes and human identity, as the evaluation dimensions. As detailed in Tab. 13, our RM outperforms both the baseline and the VideoAlign-MQ guided training. Both BT-WT and HPQA generate positive returns, with the former yielding even higher returns.

7.5.2. Semantic Alignment

Tab. 14 summarizes the performance comparison of the HunyuanVideo backbone after post-training with different reward models, evaluated on the VBench benchmark for semantic alignment. Both post-training methods, using the

VideoAlign TA reward model and our SoliReward, improve upon the baseline HunyuanVideo model’s semantic score of 0.7334. Our proposed reward model achieves the highest overall performance, with a semantic score of **0.7544**, surpassing the TA model’s score of 0.7421.

8. Data Annotation

8.1. Single-Item Binary Annotation Design

To ensure a standardized and rigorous evaluation process, we formulate detailed annotation guidelines for our human annotators. These guidelines, summarized in Tab. 15, provide a structured framework for assessing the quality of generated videos. The evaluation is organized into three primary dimensions. The first dimension, **Subject Deformity**, focuses on the structural plausibility and temporal stability of the subjects within the video. The second dimension, **Physical Plausibility**, evaluates the adherence of the video’s dynamics to real-world physical laws, including motion, gravity, and object interactions. The final dimension, **Semantic Alignment**, measures the relevance of the generated video content to the input text prompt, encompassing core semantics, detailed descriptions, and stylistic specifications. To simplify the annotation task and ensure consistency, annotators are instructed to perform a binary assessment for each dimension. They are required solely to judge whether a video passes or fails the specific criteria defined for that dimension.

8.2. Data Distribution

We collected annotations for 250k in-house videos and a 50k-sample out-of-distribution (OOD) test set generated by other SOTA models (including Wan2.1 [30], Wan2.2 [30], Veo 3 [7] and Seedance 1.0 [6]). These samples originate from 20k unique prompts. To ensure diversity, we balanced these prompts across multiple attributes including subject, motion, style, and camera control. In Fig. 7, we demonstrate the quality distribution of our in-house dataset. To construct the BT-WT dataset, we randomly selected 350k win-lose and 150k win-tie pairs based on the cross-prompt pairing strategy.

9. Implementation Details

9.1. Reward Model Training

We trained the reward model on a 4-node CentOS cluster, each node featuring 8 NVIDIA H20 GPUs with 96GB CUDA memory and an AMD EPYC 9K84 96-Core Processor. All other hyperparameters are detailed in Tab. 16.

9.2. Post-Training

We conducted post-training experiments on a 5-node CentOS cluster, each node featuring 8 NVIDIA H800 GPUs

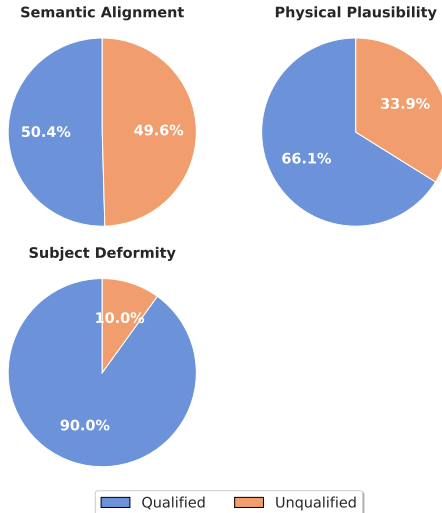


Figure 7. Quality distribution of our in-house dataset.

(80GB CUDA memory) and an Intel Xeon Platinum 8476C Processor. Key hyperparameters are detailed in Tab. 17.

10. More Visualization Results

Further visualization results are presented in Fig. 8. We also provide visual comparisons between BT and BT-WT in Fig. 9. For extensive qualitative results, please refer to the supplementary material, which includes HTML pages for convenient viewing.

Table 14. Comparison of post-training with different reward models on semantic alignment. Evaluations are conducted on VBench [10].

Backbone	RM	Scene	Consistency	Appearance	Object	Spatial	Action	Temporal	Color	Multiple	Semantic (Avg.)
HunyuanVideo	-	0.3496	0.2700	0.2021	0.8006	0.6993	0.9600	0.2539	0.8730	0.6966	0.7334
HunyuanVideo	TA	0.3895	0.2702	0.2039	0.7927	0.7150	0.9700	0.2539	0.8269	0.7477	0.7421
HunyuanVideo	Ours	0.3692	0.2678	0.1981	0.8275	0.7517	0.9700	0.2518	0.9080	0.7630	0.7544

Table 15. Definitions of the evaluation dimensions and their key assessment criteria used in our human evaluation framework.

Evaluation Dimension	Definition and Key Criteria
Subject Deformity	<p>Assesses the presence and severity of structural artifacts and temporal instability impacting subjects (e.g., humans, animals, objects).</p> <ul style="list-style-type: none"> - Structural Artifacts: Evaluates anatomical incorrectness, penalizing severe distortions, unnatural forms, or implausible subject parts (e.g., faces, limbs). - Temporal Instability: Measures inconsistencies in a subject’s identity or form, penalizing artifacts like “melting”, “flickering”, or unnatural morphing across frames.
Physical Plausibility	<p>Assesses the adherence of video dynamics to real-world physical principles.</p> <ul style="list-style-type: none"> - Motion Dynamics: Checks if object motion, acceleration, and inertia appear physically coherent and natural. - Object Interactions: Evaluates the realism of interactions with forces like gravity (e.g., falling) and between entities (e.g., collisions, splashes). - Material Dynamics: Assesses the realistic behavior and deformation of complex materials such as fluids (water, smoke) or soft bodies (cloth).
Semantic Alignment	<p>Assesses the fidelity of the generated video content with respect to the input text prompt.</p> <ul style="list-style-type: none"> - Core Semantics: Fidelity to the primary semantic components of the prompt, including the main subject, key action, and overall scene. - Detailed Attributes: Fidelity to specific descriptive details, such as subject attributes (e.g., color, appearance), action modifiers, and background elements. - Stylistic & Cinematic Fidelity: Alignment with specified artistic styles (e.g., 3D render) and cinematic instructions (e.g., camera motion, “close-up”).

Table 16. Implementation details for reward model training.

Hyperparameter	Value
Model	InternVL3-1B/8B/14B
Distributed Training	DeepSpeed Stage 0/3/3
Trainable Parameters	Full
Learning Rate	1e-6
Num. Train Epochs	3.0
Per Device Train Batch Size	1
Gradient Accumulation Steps	10
Optimizer	AdamW
Adam β_1	0.9
Adam β_2	0.999
Weight Decay	0.01
LR Scheduler	linear
Warmup Ratio	0.05
Reward Margin	3.0
Precision	BF16
Gradient Checkpointing	True

Table 17. Implementation details for post-training.

Hyperparameter	Value
Base Model	HunyuanVideo 14B
Trainable Parameters	Full
Learning Rate	1e-6
Per Device Train Batch Size	1
Gradient Accumulation Steps	4
Max Train Steps	500
LR Scheduler	constant with warmup
LR Warmup Steps	0
Mixed Precision	bf16
Gradient Checkpointing	True
SDE η	0.25
Video Resolution (train)	480 × 480
Video Frames (train)	32
Video FPS (train)	8
Denoising Steps (train)	16
Time Shift (train)	5.0
Video Resolution (test)	640 × 640
Video Frames (test)	91
Video FPS (test)	18
Denoising Steps (test)	30
Time Shift (test)	7.0
Group Size	8
Distributed Training	FSDP FULL SHARD

A man with red hair sits on a couch, holding a bowl of chips and a bottle.

Baseline



VideoAlign



Ours

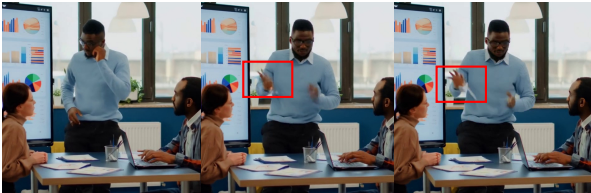


A young woman with an afro hairstyle waves while holding a smartphone.



A group of people sit around a table with laptops, looking at data visualizations.

Baseline



VideoAlign



Ours



A man with a shaved head is doing squats on an orange yoga mat.

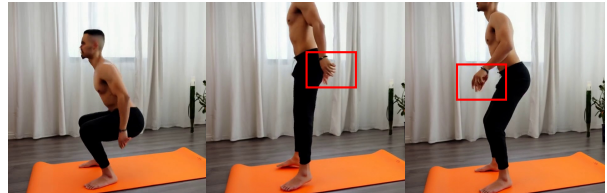
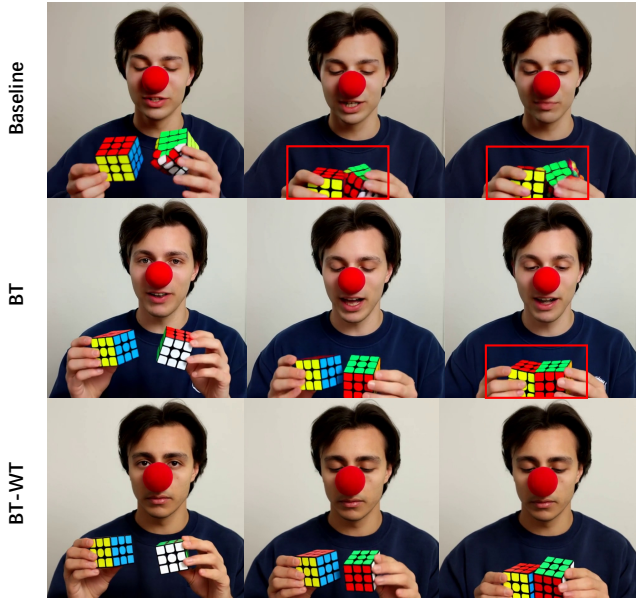


Figure 8. More visualization results guided by VideoAlign and SoliReward.

A person with a red nose holds two Rubik's Cubes.



A woman sits at a desk with papers, holding up signs that say "LESSON 1" and "3+7"



A woman arranges bread on a wooden stand.



A man pours liquid from a red can into a black container.



Figure 9. Visualization results guided by BT and BT-WT.